Modeling of Turbulent Cross Flow Microfiltration of Pomegranate Juice Using Hollow Fiber Membranes

Sourav Mondal and Sirshendu De
Dept. of Chemical Engineering, Indian Institute of Technology Kharagpur, Kharagpur 721302, India

Alfredo Cassano and Franco Tasselli
Inst. on Membrane Technology, ITM-CNR, c/o University of Calabria, via P. Bucci, 17/C, I-87030 Rende, Cosenza, Italy

DOI 10.1002/aic.14594
Published online August 27, 2014 in Wiley Online Library (wileyonlinelibrary.com)

A mathematical analysis of the permeate flux decline during microfiltration of fruit juice with hollow fibers under turbulent flow is presented. Impact of complex fluid flow phenomena on mass transfer is analyzed. A comprehensive analytical model for developing concentration boundary layer was formulated from first principles using integral method. Attempts to model the system considering constant boundary layer thickness (film theory) is inaccurate for developing boundary layer. Gel resistance parameter depending on juice characteristics has significant impact on permeate flux. Specific gel layer concentration has insignificant effect on system performance under total recycle mode but important for batch mode. Theoretical results were compared with experiments in clarification of pomegranate juice with poly(ether ether ketone) and polysulfone hollow fiber membranes. The physical parameters of complex mixture were evaluated by optimizing of the flux profiles in total recycle mode of operation and were successfully applied for prediction of batch mode performance. © 2014 American Institute of Chemical Engineers *AIChE J*, 60: 4279–4291, 2014
Keywords: hollow fiber membranes, microfiltration, pomegranate juice, mathematical modeling, transport phenomena

Introduction

Membrane-based separation processes, such as microfiltration (MF) and ultrafiltration (UF), are used in the clarification of fruit juices and processing of food products as they do not involve chemical additives and thermal degradation. In addition, these processes reduce processing time and operating cost and make some conventional unit operations, like fining treatment, centrifugation, and polish filtration redundant.

MF and UF are widely used to clarify fruit juices.[1] The clarified juice is a heat-sensitive solution containing lower molecular weight compounds including flavors, acids, and sugars and has reasonably high shelf life.[2] Application of these processes to clarify various fruit and vegetable juice has been extensively studied during the last 30 years. Some examples are clarification of mosambi,[3] apple,[4,5] banana,[6] passion fruit,[7] sugarcane,[8] pineapple,[9,10] orange,[11,12] cactus pear,[13] carrot,[14] kiwifruit,[15]and pomegranate[16,17] juice.

Fruit juice is a complex mixture of several components in the solution. As it contains high molecular weight proteins, fibers, cellulose, and so forth, the separation process is primarily gel layer controlled.[9] There have been several attempts reported in literature to apply resistance in series and pore blocking models to predict the flux decline behavior.[2,4,15] However, such models lack the physical understanding of the process necessary to capture the variation in feed characteristics and are mostly empirical in nature.

The flow characteristics in hollow fiber membrane module have significant effect on the mass transfer analysis. The flow regime determines the extent of mass transport and permeate flux. Mass transfer analysis in the laminar flow for hollow fiber membrane system has already been carried out for gel controlling filtration,[18] osmotic controlled filtration with[19] and without suction.[20] It has been found that the developing mass transfer boundary layer model gives more realistic prediction than the constant mass transfer boundary layer.

The mass transfer analysis in turbulent flow regime for hollow fiber membranes was reported by few researchers.[21–23] Parvatiyar carried out this analysis using spectral theory for both newtonian and non-newtonian rheologies[21] and the turbulence was quantified for the all the three zones. However, the entire analysis was carried out for impervious conduit without any permeation. Estimation of the mass-transfer coefficient in turbulent regime with permeation was performed by Minikanti et al.[22] They have incorporated the phenomena of suction for Newtonian fluids. The effect of suction on the mass transfer of UF under turbulent flow regime was illustrated for the first time in this work. An extended version of this study was performed by Ranjan et al.,[23] considering the effects of non-newtonian rheology. The effect of rheology ranging from pseudoplastic to dilatant

Correspondence concerning this article should be addressed to S. De at sde@che.iitkgp.ernet.in.

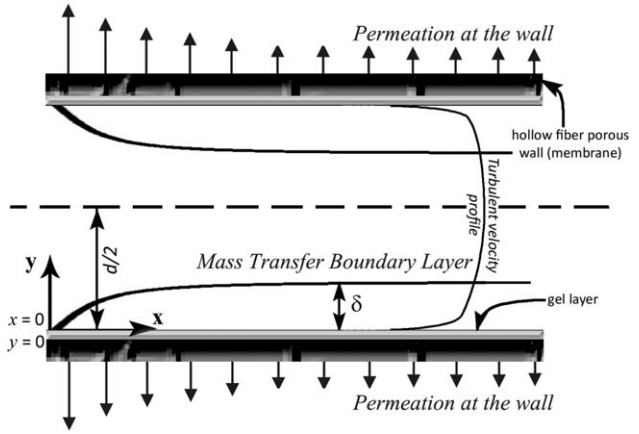

Figure 1. Schematic of the model geometry inside the hollow fiber membrane.

on the Sherwood number was presented in this work. Predictive modeling of cross flow UF under turbulent conditions was reported by Sreenivas et al.[24] The system performance in terms of the permeate flux and permeate concentration was predicted. The model results were also compared with the experimental data for UF of NaCl and dextran. However, this study was carried out in a rectangular channel.

All the above analyses related to mass transfer in membrane system under turbulent flow conditions were performed for osmotic pressure controlling filtration. However, a comprehensive model with gel layer controlled filtration under turbulent conditions in hollow fibers has not been reported in literature.

The present model attempts to quantify the flux decline behavior during MF of fruit juice in hollow fiber under turbulent flow conditions. The mathematical analysis was based on the first principles using the integral method of solution to compute the developing concentration boundary layer over the gel layer. The analysis was extended for batch mode of filtration, and the profiles of permeate flux were computed for different operating conditions in the predictive mode. The simulated results were also compared with the experimental data obtained in the clarification of pomegranate juice with modified poly(ether ether ketone) (PEEK-WC) and polysulfone (PSU) hollow fiber membranes prepared in laboratory. The physicochemical parameters of such complex liquid mixture were evaluated by optimizing of the flux profiles in total recycle mode of operation.

Theoretical Methodology

The schematic of the development of mass transfer boundary layer in the hollow fiber along with the geometry and co-ordinate system is presented in Figure 1. The complex nature of the fluid flow during turbulent conditions can be represented by piecewise polynomial expression of velocity for different zones (viscous sublayer, buffer zone, and turbulent core) of the turbulent velocity profile.[25] However, this adds to the mathematical complexity during the integral solution of the mass transfer boundary layer, as it would require integration in different regions of y co-ordinate resulting in different nature of the mass transfer boundary layer thickness. Thus, a single velocity field expression representing all regions of the flow field is desirable as proposed by Reichardt.[26] The fully developed steady state turbulent velocity profile for flow through closed conduit can be expressed in terms of the co-ordinate system fixed at the walls as[26]

$$u^+ = \frac{1}{\lambda}\ln\left(1+\lambda y^+\right)+7.8\left[1-\exp\left(-\frac{y^+}{11}\right)-\frac{y^+}{11}\exp\left(-0.33y^+\right)\right] \tag{1}$$

where, λ is the von-Karman constant equal to 0.41 [26]; y^+ is nondimensional transverse dimension $\left(=\frac{u*}{\mu/\rho}y\right)$; $u^+ = \frac{u}{u*}$; u^* is friction velocity $\left(=\sqrt{\tau_w/\rho}\right)$; and wall shear stress τ_w is expressed as[27]

$$\tau_w = 0.03954\rho u_0^2\left(\frac{\mu}{\rho u_0 d}\right)^{0.25} \tag{2}$$

The velocity profile in Eq. 1 is applicable for both the viscous sublayer and buffer zone of the turbulent flow. During MF of fruit juice, the suspended solids are completely rejected forming a gel-type layer over the membrane surface. Due to this, there exists a concentration boundary layer next to the gel layer with a variation in concentration from bulk to gel concentration. The species transport equation for gel forming solute within the concentration boundary layer, for a tubular module is given as

$$\underbrace{\frac{\partial c}{\partial t}}_{T_1} + \underbrace{u\frac{\partial c}{\partial x}}_{T_2} + \underbrace{v\frac{\partial c}{\partial r}}_{T_3} = \underbrace{\frac{D}{r}\frac{\partial}{\partial r}\left(r\frac{\partial c}{\partial r}\right)}_{T_4} \tag{3}$$

The major assumptions in this analysis are: (1) Considering an order of magnitude analysis term wise using typical dimensional scales, $O(r) \approx 10^{-6}$; $O(x) \approx 10^{-1}$; $O(v) \approx 10^{-5}$; $O(D) \approx 10^{-11}$; $O(c) \approx 10^{1}$; $O(t) \approx 10^{2}$; and $O(u) \approx 1$, one can understand that $O(T_1) \approx 10^{-1}$; $O(T_2) \approx 10^{2}$; $O(T_3) \approx 10^{2}$; and $O(T_4) \approx 10^{2}$. Thus, it may be noted that the order of magnitude of T_1 is significantly less than the rest of the terms, which reduces further for longer filtration duration (above 1000 s). Therefore, we can take recourse to quasi steady-state analysis for estimation of concentration boundary layer profile, ignoring T_1; (2) The cross flow velocity is much higher compared to the permeation velocity. Therefore, the axial velocity profile is not distorted due to permeation; (3) mass transfer boundary layer is typically less than 10% of the internal diameter of the tube. Thus, the effect of wall curvature can be neglected and r co-ordinate in Eq. 3 can be converted to a planar one starting from the tube wall[28] as $y = (d/2) - r$; (4) As, the mass transfer boundary layer thickness is extremely small, it can be assumed that the y-component velocity is equal to the permeation velocity at the wall.[29] Therefore, the y-component velocity becomes

$$v = -v_w \tag{4}$$

Based on the above assumptions, Eq. 3 can be written as

$$u\frac{\partial c}{\partial x} - v_w\frac{\partial c}{\partial y} = D\frac{\partial^2 c}{\partial y^2} \tag{5}$$

Following nondimensional variables are defined for the rest of the analysis

$$U=\frac{u}{u_0};\ Y=\frac{y}{d};\ C=\frac{c}{c_0};\ X=\frac{x}{L};\ \mathrm{Re}=\frac{\rho u_0 d}{\mu};\ Pe_w=\frac{v_w d}{D}\ \text{and}\ Sc=\frac{\mu}{\rho D}$$

The turbulent velocity profile (Eq. 1) in terms of nondimensional variables is expressed as

$$U=\begin{pmatrix}0.5\ln\left[1+0.082\,\mathrm{Re}^{0.875}Y\right]+\\1.56\left[1-\exp\left(-0.018\,\mathrm{Re}^{0.875}Y\right)-0.018\,\mathrm{Re}^{0.875}Y\exp\left(-0.066\,\mathrm{Re}^{0.875}Y\right)\right]\end{pmatrix}\mathrm{Re}^{-0.125} \tag{6a}$$

Defining $P=0.5\,\mathrm{Re}^{-0.125}$; $Q=0.082\,\mathrm{Re}^{0.875}$; $R=1.56\,\mathrm{Re}^{-0.125}$; $S=0.018\,\mathrm{Re}^{0.875}$; $T=0.066\,\mathrm{Re}^{0.875}$, the above equation is transformed as

$$U=P\ln\left[1+QY\right]+R\left[1-\exp\left(-SY\right)-SY\exp\left(-TY\right)\right] \tag{6b}$$

Similarly, the species transport equation is made nondimensional

$$\mathrm{Re}\,Sc\frac{d}{L}U\frac{\partial C}{\partial X}-Pe_{\mathrm{w}}\frac{\partial C}{\partial Y}=\frac{\partial^2 C}{\partial Y^2} \tag{7}$$

The solution of the Eq. 7 is attempted using an integral method. A quadratic concentration profile which is the simplest way to express the concentration profile in the boundary layer that satisfies three boundary conditions presented subsequently. Thus, the concentration profile within mass transfer boundary layer is assumed

$$C=a_0+a_1Y+a_2Y^2 \tag{8}$$

where, a_0, a_1, and a_2 are the constant coefficients. Using the following boundary conditions for the concentration profile within the mass transfer boundary layer, the constants can be evaluated,

$$\text{at } Y=0,\ C=C_{\mathrm{g}}\left(=c_{\mathrm{g}}/c_0\right) \tag{9a}$$

$$\text{at } Y=\Delta\left(=\delta/d\right),\ C=1 \tag{9b}$$

$$\text{at } Y=\Delta\left(=\delta/d\right),\ \frac{d\Delta}{dY}=0 \tag{9c}$$

Thus, the concentration profile is obtained as

$$C=C_{\mathrm{g}}-2\left(C_{\mathrm{g}}-1\right)\left(\frac{Y}{\Delta}\right)+\left(C_{\mathrm{g}}-1\right)\left(\frac{Y}{\Delta}\right)^2 \tag{10}$$

Calculating the partial derivatives $\frac{\partial C}{\partial X}$, $\frac{\partial C}{\partial Y}$, $\frac{\partial^2 C}{\partial Y^2}$ and substituting them in Eq. 7, the following equation is obtained

$$\mathrm{Re}\,Sc\frac{d}{L}\left(\frac{Y}{\Delta^2}-\frac{Y^2}{\Delta^3}\right)U\frac{d\Delta}{dX}-Pe_{\mathrm{w}}\left(\frac{Y}{\Delta^2}-\frac{1}{\Delta}\right)=\frac{1}{\Delta^2} \tag{11}$$

Taking the zeroth moment (multiplying both sides by $\mathrm{Y}^0\mathrm{dY}$ and integrating term by term over the boundary thickness) of the above equation[18] and integrating across the thickness of the boundary layer (0 to Δ), the following differential equation is resulted

$$\mathrm{Re}\,Sc\frac{d}{L}\Delta\frac{d\Delta}{dX}I_1-\frac{1}{2}Pe_{\mathrm{w}}\Delta=1 \tag{12}$$

where,

$$I_1=\int_0^{\Delta}U\left(\frac{Y}{\Delta^2}-\frac{Y^2}{\Delta^3}\right)dY$$

$$=\int_0^{\Delta}\left\{P\ln\left[1+QY\right]+R\left[1-\exp\left(-SY\right)-SY\exp\left(-TY\right)\right]\right\}\left(\frac{Y}{\Delta^2}-\frac{Y^2}{\Delta^3}\right)dY \tag{13}$$

The above integration is evaluated term wise and the complete algebraic expression of I_1 is presented in the Appendix A.

Now, considering a steady-state mass balance over the membrane surface ($y=0$), the following equation is obtained

$$v_{\mathrm{w}}c_{\mathrm{g}}+D\frac{\partial c}{\partial y}=0 \tag{14}$$

The above equation physically indicates net flux (convective flux towards and diffusive flux away from the membrane surface) towards the membrane equals zero at steady state. In nondimensional terms, the above equation can be represented as

$$Pe_{\mathrm{w}}C_{\mathrm{g}}+\frac{\partial C}{\partial Y}=0 \tag{15}$$

Substituting the expression of $\frac{\partial C}{\partial Y}$ from Eq. 10, we get

$$\frac{1}{2}Pe_{\mathrm{w}}\Delta=1-\frac{1}{C_{\mathrm{g}}} \tag{16}$$

Equation 12 is modified by incorporating Eq. 16 as

$$\frac{d\Delta}{dX}=\frac{1}{I_1C_{\mathrm{g}}\left(\mathrm{Re}\,Sc\frac{d}{L}\right)\Delta} \tag{17}$$

The initial condition of Eq. 17 is at $X=0$, $\Delta=0$. However, this condition leads to numerical instability due blowing off as triangle appears in the denominator of Eq. 17, and therefore, an asymptotic solution for $\Delta(\text{at } X\to 0)$ is derived.

In the limit of $X\to 0$, $Y<<1$, and thus, Y^2 and higher order terms are neglected. Under this limit, the expression of U (as in Eq. 6) becomes

$$U=PQ\ Y=0.041\,\mathrm{Re}^{0.75}Y \tag{18}$$

Note that the terms $\ln\left[1+QY\right]$, $\exp\left(-SY\right)$, and $\exp\left(-TY\right)$ in Eq. 6b are expanded in the limit of $Y<<1$ to obtain the above simplified velocity equation. Substituting this expression of U in Eq. 7 and proceeding exactly as above, a closed form initial solution of Δ is obtained

$$\Delta=9.57\left(\frac{X}{\mathrm{Re}^{1.75}Sc\frac{d}{L}C_{\mathrm{g}}}\right)^{1/3} \tag{19}$$

To avoid the numerical instability, the initial condition for Eq. 17 is considered that at a small value of X (say 10^{-4}), Δ is computed using Eq. 19.

Estimation of the mass-transfer coefficient

The definition of the mass-transfer coefficient (k) can be written as

$$k\left(c_{\mathrm{g}}-c_0\right)=-D\frac{\partial c}{\partial y}\Big|_{y=0} \tag{20}$$

Substituting the expression of $\frac{\partial c}{\partial y}|_{y=0}$ and nondimensionalizing the above equation, we get

$$Sh = \frac{kd}{D} = \frac{2}{\Delta} \tag{21}$$

As, Δ is the function of the length of the membrane, the length averaged Sherwood number becomes

$$\overline{Sh_L} = \int_0^1 Sh(X)dX = 2\int_0^1 \frac{dX}{\Delta} \tag{22}$$

Total recycle mode of operation

In the total recycle mode, the permeate is recycled back to the feed. Thus, the feed concentration remains invariant with time. This is a popular mode of membrane filtration and is used to study the effects of cross flow velocity and other operating parameters. To quantify the permeate flux, the mass-transfer coefficient as calculated earlier is used. Considering a material balance equation for the gel-forming component in the concentration boundary layer[30]

$$\text{mass flux} = \rho_g(1-\varepsilon_g)\frac{dH}{dt} = v_w c - D\frac{dc}{dy} \tag{23}$$

subjected to the boundary conditions

$$\text{at } y=0, \quad c=c_0 \tag{24a}$$

$$\text{at } y=\delta, \quad c=c_g \tag{24b}$$

Initial condition of Eq. 23 is

$$\text{at } t=0, \; H=0 \tag{24c}$$

Solving the above equation in the y-direction, satisfying the boundary conditions and replacing D/δ as $\overline{k_L}$, Eq. 23 becomes

$$\rho_g(1-\varepsilon_g)\frac{dH}{dt} = v_w \frac{c_0 - c_g \exp(-v_w/\overline{k_L})}{1-\exp(-v_w/\overline{k_L})} \tag{25}$$

where, $\overline{k_L}$ is the length averaged mass-transfer coefficient obtained from $\overline{Sh_L}$ (Eq. 22). It must be noted here, that the above equation transforms into the classical form at steady state

$$v_w = \overline{k_L} \ln \frac{c_g}{c_0} \tag{26}$$

The permeate flux satisfies the help of the phenomenological Darcy's equation

$$v_w = \frac{\Delta P}{\mu(R_m + R_g)} \tag{27}$$

where, R_g is the gel resistance dependent on the gel density, thickness, porosity, and specific gel resistance, which is described as[18]

$$R_g = \beta(1-\varepsilon_g)\rho_g H = \xi H \tag{28}$$

where, $\xi = \beta(1-\varepsilon_g)\rho_g$. Fruit juice containing high amount of suspended solids, fiber, pectin, and so forth, are likely to exhibit higher magnitude of β. The value of gel layer density (ρ_g) typically varies between 1400 and 1800 kg/m^3 for membrane filtration of citrus fruit juices. It can be mentioned here that during the experiment, the effective fiber diameter is reduced due to the formation of the gel layer, thereby affecting the velocity. Consequently, the linear cross flow velocity is increased as

$$u_0 = \frac{Q_F}{\pi n(d-2H)^2} \tag{29}$$

where, Q_F is cross flow rate. Thus, Eqs. 22, 25, and 27–29 become a set of coupled differential algebraic equations which is solved numerically using the fourth order Runge–Kutta method, thereby, resulting to profiles of gel layer thickness and permeate flux. The algorithm for calculation is presented in Appendix B.

Optimization of the model parameters

The physical properties of the system are gel porosity (ε_g), gel density (ρ_g), specific gel resistance parameter (ξ), diffusivity of the gel forming solute (D), and gel concentration (C_g). However, quantification of these properties for complex mixture such as fruit juice are difficult to estimate experimentally. Thereby, the values of these parameters are computed by constrained optimization of the experimental flux profiles in case of total recycle mode with model results. This is done by minimizing the sum of the square of the relative error between the experimental and simulated data at the same time point using an interior point optimization algorithm.[31] The optimality of the optimization constraint takes into account the Karush–Kuhn–Tucker condition that the gradient must be zero at a minimum modified to consider the constraints.[32] The values of the physical parameters are limited by the upper and lower constraints. As, the model is applied for clarification of fruit juice systems by MF, the rejected solutes are expected to have low diffusivities. Thus, the magnitude of the diffusivity (D) is bounded with (1 to 9) $\times$ 10^{-12} m^2/s in the optimization algorithm. The value of c_g/c_0 is limited with 3.0 to 6.0, as the gel layer density is not high enough and lies within 1400 to 1800 kg/m^3. Considering an order of magnitude analysis of the permeate flux, the gel layer resistance parameter (ξ) is found to be bounded within (0.5 to 5) $\times$ 10^{17} m^{-2}. Thus, within the constraints to be satisfied, by each of the variables, the optimization yielded a unique solution set of parameters considering a tolerance of 0.01 for the objective function. The objective function, defined as the sum of square of error (Err) between the experimental and predicted flux values for all operating conditions and time points is given as

$$\text{Err} = \sum_{i=1}^{n}\sum_{j=1}^{k}\left(\frac{v_{w,cal}^{i,j} - v_{w,\exp}^{i,j}}{v_{w,\exp}^{i,j}}\right)^2 \tag{30}$$

where, i is number of experiments and j is number of time points in the i-th experiment.

Batch mode of operation

In this mode of operation, the permeate is continuously withdrawn from the system, unlike the total recycle mode. As a result, the feed concentration of the completely rejecting solute increases with time. Considering an overall mass balance, the rate of volume reduction is represented as

$$\frac{d}{dt}(\rho_f V) = -v_w A_m \rho_p \tag{31}$$

where, ρ_f and ρ_p are the densities of the feed and permeate, respectively. The difference in the feed and permeate densities are insignificant when the total solids content in the feed is less than 30% w/v. Assuming there is negligible change in density between feed and permeate, Eq. 31 is modified as

$$\frac{dV}{dt} = -v_w A_m \tag{32}$$

Now, considering an overall species balance of the gel forming solute, the rate of change of the feed concentration

Table 1. Characteristics of Hollow Fiber Membranes[33]

Membrane material	PEEK-WC	PSU
Internal diameter (mm)	1.19	1.43
External diameter (mm)	1.62	1.73
Thickness (mm)	0.215	0.15
Hydraulic permeability (L/m^{2}hbar)	536.14	654.81
Largest pore diameter (μm)	0.442	0.432
Mean pore diameter (μm)	0.140	0.137

is presented as (assuming gel forming solute is completely rejected by the membrane)

$$\frac{d}{dt}(c_b V) = -v_w A_m c_p = 0 \tag{33}$$

Thus, the above equation is simplified to

$$c_b V = c_0 V_0 \tag{34}$$

The above equation can be used to directly estimate the feed concentration at any point of time during the membrane filtration. Following a similar analysis as in the case of total recycle mode, the differential equation for the thickness of the gel layer (refer to Eq. 25) is modified as

$$\rho_g(1-\varepsilon_g)\frac{dH_b}{dt} = v_w \frac{c_b - c_g \exp(-v_w/\overline{k_L})}{1-\exp(-v_w/\overline{k_L})} \tag{35}$$

Thus, Eqs. 22, 27–29, 32, 34, and 35 becomes a set of coupled system of differential algebraic equations which is solved numerically using the fourth order Runge–Kutta method resulting to variation of gel layer thickness, permeate flux, volume, and concentration of solutes in the feed as a function of time. In this case, the numerical algorithm is similar to that presented in Appendix B. The only difference is the optimization has been omitted as the system parameters used are already obtained from total recycle mode calculation. Therefore, the model result is this case is entirely in predictive mode.

Experimental

Membrane preparation

Modified polyether ether ketone (PEEK-WC) and PSU hollow fiber membranes were prepared according to the dry-wet spinning technique.[33] Their characteristics are reported in Table 1. The average pore size of the prepared membrane is measured using capillary porometer. Membrane modules were prepared by embedding four hollow fiber membranes inside a 20-cm long glass tube (effective membrane length 18 cm) with epoxy resin. Total membrane surface area was calculated as 26.9 and 32.3 cm^2 for the PEEK-WC and PSU hollow fiber membrane modules, respectively.

Table 2. Physicochemical Characteristics of Unclarified Pomegranate Juice[33]

Suspended Solids (%w/w)	4.1
Total soluble solids (g/100 g)	16.0
pH	3.7
Viscosity (mPa s)	1.5
Total acidity (% citric acid)	0.43
Total phenols (g catechin/L)	1.57
Total organic carbon (TOC) (g/L)	53.2
Citric acid (g/L)	1.47
Malic acid (g/L)	1.90
Ascorbic acid (mg/L)	68.0

Juice characteristics

Pomegranate juice obtained from fruits of Sicilian origin (*Punica granatum* cv*Selinunte*) was supplied by Citrech Snc (Messina, Italy). Raw juice was kept frozen at −17°C and defrosted before use. Physicochemical characteristics of unclarified juice are reported in Table 2 which includes total organic carbon, acorbic acid, citric acid, and mallic acid. The suspended solids concentration is taken as the feed concentration for the model.

MF unit and procedures

Pomegranate juice was clarified using a laboratory plant unit (DSS LabUnit M10) supplied by Danish Separation System AS, Denmark. The equipment consisted of a feed tank, a thermometer, a cross-flow pump (ECO type GA4-KDT-TTU), two manometers for the measurement of the inlet and outlet pressures, a pressure control valve, and a multitube heat exchanger fed with tap water. The feed temperature was controlled by circulating cooling water through the heat exchanger. Transmembrane pressure (TMP) was controlled by the valve on the retentate side and by setting the speed of the pump. A schematic representation of the experimental setup is depicted in Figure 2.

MF experiments were performed according to the total recycle and batch concentration configurations. In the former, the permeate was continuously recycled to the feed tank to ensure constant volume and composition of the feed. For each set of experiments, two parameters were fixed and the other was varied to cover the ranges indicated in Table 3. The permeate flux was measured every 5 min for 2 h. In the batch concentration configuration, the MF system was operated in selected operating conditions (Table 3) so that the final volume reduction factor (VRF) was 2.

At the end of each run, a cleaning-in-place protocol using distilled water and NaClO solution (4 g/L, 40°C, 60 min) was used to restore the original water flux. The chemical structures of the PEEK-WC and PSU polymer are presented in Figure 3. Now there exist possibilities of the chemical modification of the polymer (PEEK-WC) unit by—oxidation of the keto group, electrophillic substitution at *ortho* or *para*

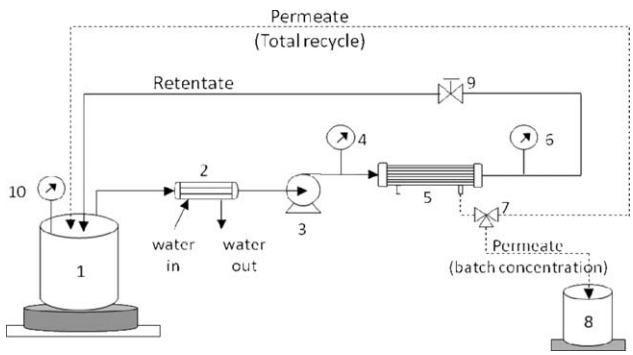

Figure 2. Schematic of the experimental setup: (1) feed tank; (2) heat exchanger; (3) feed pump; (4,6) manometers; (5) membrane module; (7) three-way valve; (8) permeate tank; (9) pressure control valve; (10) thermometer.

Table 3. Operating Conditions in Total Recycle and Batch Concentration Configurations[33]

	Configuration	
Membrane Type	Total Recycle	Batch Concentration
PEEK	$Q_F = 63$ l/h TMP = 0.6 bar; $T = 25°C$	TMP = 1.15 bar $Q_F = 59$ l/h $T = 25°C$
PS	$Q_F = 98$ l/h TMP = 0.65 bar; $T = 25°C$	TMP = 1.55 bar $Q_F = 68$ l/h $T = 25°C$

positions of the benzene rings and reaction of the keto group with hydrazines to form imines. The oxidation reaction requires strong chemical environment (presence of hydroperoxides, per-acid, UV treatment, etc.)[34] which is not available with fruit juice mixtures. Electrophilic substitutions are possible only in presence of electrophiles. Reactions with hydrazines are not feasible as hydrazines are absent in fruit juices. As the permeability of the membranes are regained by washing with weak acidic solution (NaClO), it is confirmed that no chemical reaction/modification of the keto group or benzene ring of the polymer occurs which cannot be reversed by NaClO solution. The role of NaClO solution is just to provide a mild acidic environment to redissolve the fruit juice components which have fouled the membrane surface or inside the pores and to break the hydrogen bonding between molecules, if any.[35,36] The PSU unit is comparatively more inert compared to PEEK. The presence of sulphonated keto group and tertiary carbon makes it chemically stable and inert. Chemical reactions with the PSU unit are highly improbable in fruit juice environment. Thus, in this case, cleaning of the membrane is achieved in mild acidic NaClO solution.

Results and Discussion

Membrane fouling is an important aspect in filtration. The different types of fouling can be broadly categorized as concentration polarization like cake/gel layer formation (reversible fouling) and irreversible fouling such as complete, intermediate, and standard pore blocking. A single fouling mechanism or simultaneous occurrences of multiple mechanisms are also possible.[37,38] The deposition of the solutes over the membrane surface is due to concentration polarization, gel layer formation and pore blocking. Transport model to predict the membrane filtration performance considering the surface and internal fouling for waste water treatment was reported by Tu et al.[39,40] Their results show that presence of natural organic matter (NOM) is a potential foulant. Also, the membrane material has an important role which affects the concentration boundary layer thickness and gel layer formation. Increase in TMP increases the internal pore fouling. Enhancement of the cross flow rate or turbulence decreases the hydrodynamic resistances and thickness of mass transfer boundary layers, which is similar to the presence scenario with MF of fruit juices. Biological fouling due to the presence of biodegradable organic matter (BOM) in fruit juice is an important aspect in membrane filtration. Membrane bioreactor is useful for reduction of the biodegradable organic components from water. Removal of aldehydes as high as 98–99% was possible using MF or UF along with powder activated carbon as preadsorption and biodegradation.[41] Modeling of such systems for design and upscaling of such membrane bioreactor processes is also done taking into account the biofouling and biodegradation.[42] Bacterial growth is another important issue is membrane filtration of real life streams. Microbiological growth due to the presence of organic carbon in solution spoils the membrane modules with prolonged usage. The presence of assimilable organic carbon (AOC) and BOM affects the bacterial and other microbial growth considerably.[43] In such systems, where AOC is content is high, pretreatment using chlorine or lime-softening is required to prevent microbial growth exceeding acceptable limits. Rejection of AOC using nanofiltration membranes shows that membrane surface charge plays a crucial role. The surface charge of the membrane is masked by increased hardness, ionic strength, and low pH of the solution, thereby reducing AOC rejection.[44] In case of fruit juices having low pH (acidic), the rejection of AOC is difficult using nanofiltration membranes. Conversely, nanofiltration removes most of the BOM. Addition of acid to prevent membrane fouling reduces the rejection of AOC for both nanofiltration and reverse osmosis membrane. Thus, prevention of microbial fouling by increasing rejection of AOC is an important is membrane filtration of fruit juice mixtures, as these contain significant proportion of dissolved organic carbon and BOM. In a complex mixture like fruit juice, there occurs large number of foulants including NOM, BOM, AOC as well as pectin, cellulose, fibers, suspended solids, and so forth, which are likely to form a gel type of layer over the membrane surface that grows with of operation leading to a decrease in throughput of the system. In this work, an attempt has been made to quantify the system performance under gel layer (formed by all components) controlled filtration.

The gel-forming components present in the pomegranate juice are mainly represented by suspended solids which are completely rejected by the MF membranes. The juice viscosity (1.5 mPa s) did not change significantly during MF. All the simulation results are referred to the physical characteristics of pomegranate juice and dimensions of the PEEK-WC hollow fiber membrane module, as described in the preceding section.

Total recycle mode

The effect of Reynolds number on the profiles of mass transfer boundary layer and Sherwood number is presented in Figure 4. From the figure, it is evident that the mass

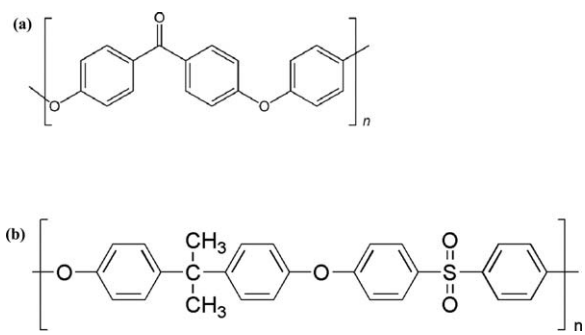

Figure 3. Chemical structures of the (a) PEEK-WC and (b) PSU polymer.

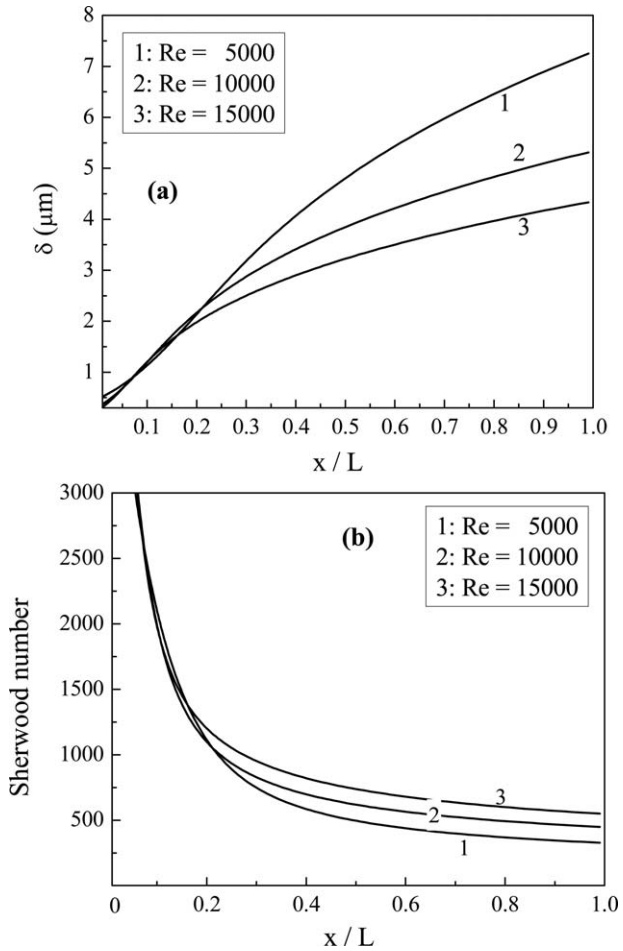

Figure 4. (a) Profile of δ with *Re*, in total recycle mode (PEEK-WC membrane and values of the physical parameters are $\rho_g = 1400$ kg/m^3; $\varepsilon_g = 0.3$; $D = 5 \times 10^{-11}$ m^2/s; $C_g = 3.2$; $\xi = 1.5 \times 10^{17}$ m^{-2}). (b) Profile of Sherwood number with *Re* as parameter in total recycle mode of operation (PEEK-WC membrane and values of the physical parameters are $\rho_g = 1400$ kg/m^3; $\varepsilon_g = 0.3$; $D = 5\text{x}10^{-11}$ m^2/s; $C_g = 3.2$; $\xi = 1.5 \times 10^{17}$ m^{-2}).

transfer boundary layer is in the developing state for this length of the module. Hence, the application of the conventional heat and mass transfer analogies, which considers fully developed boundary layer, for prediction of the Sherwood number, would seriously undermine the permeate flux in this case. The thickness of the mass transfer boundary layer is affected by the turbulence in the flow channel. It decreases with enhanced turbulence. As the Reynolds number increases, the forced convection (or turbulence) restricts the growth of mass transfer boundary layer. For example, at the end of the hollow fiber, thickness of mass transfer boundary layer decreases from 7 μm to 4.5 μm as *Re* increases from 5000 to 15000. The effect of *Re* number on Sherwood number profile are shown in Figure 3b. It is apparent from this figure that Sherwood number profiles have inverse trend of thickness of mass transfer boundary layer confirming the theory. The Sherwood number (mass-transfer coefficient) decreases sharply up to $x/L = 0.2$ due to the rapid growth of mass transfer boundary layer and stabilizes thereafter. Therefore, one can expect higher permeation rate for module lengths less than 20% of the present experimental module. Sherwood number increases with Reynolds number indicating decrease in thickness of mass transfer boundary layer with Reynolds number, resulting to less resistance offered to solvent flux across the membrane.

Effects of various parameters on permeate flux and gel layer thickness at steady state as a function of Reynolds number is presented in Figure 5. It is observed from Figure 5a, that steady-state flux increases with Reynolds number. As discussed earlier, flow turbulence reduces the mass transfer resistance as well as the gel layer thickness, resulting to enhancement in permeate flux. Effects of diffusivity on permeate flux is apparent from Curves 1 and 2. Higher diffusivity enhances mass transfer by directly increasing the mass-transfer coefficient $\left(=\frac{D}{\delta}\right)$, leading to increase in flux. Presence of low molecular weight solutes in the fruit juice mixture increases its diffusivity. Also, diffusivity is dependent

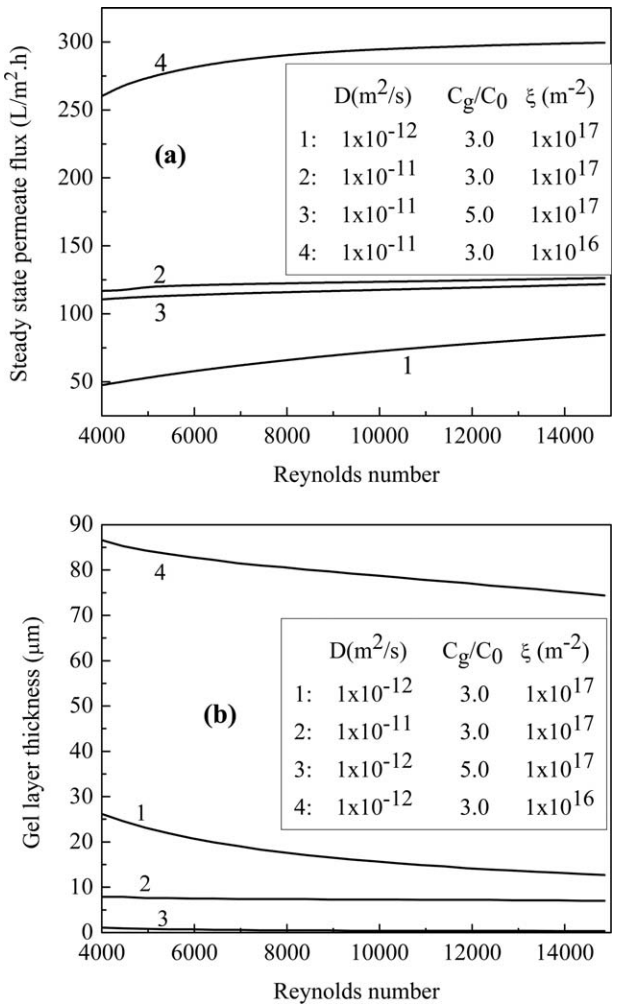

Figure 5. (a) Variation of steady-state flux with Reynolds number for different set of parameters in total recycle mode (PEEK-WC membrane and values of the physical parameters are $\rho_g = 1400$ kg/m^3; $\varepsilon_g = 0.3$). (b) Variation of the gel layer thickness with Reynolds number (PEEK-WC membrane and values of the physical parameters are $\rho_g = 1400$ kg/m^3; $\varepsilon_g = 0.3$).

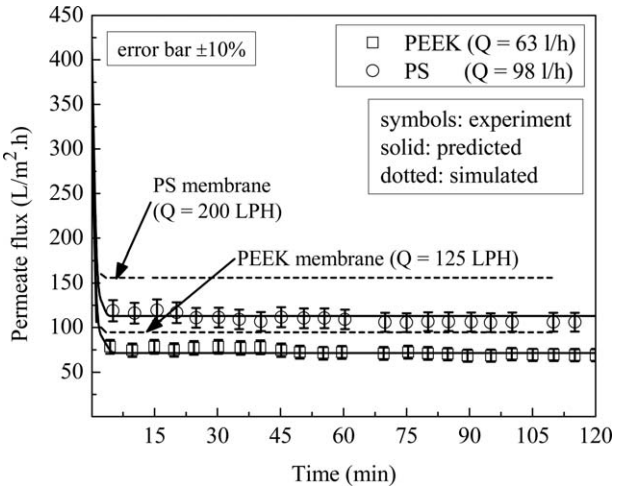

Figure 6. Comparison of the permeate flux profile with experimental and theoretical results.

The dotted lines are for simulated results of two different cross flow velocities (optimized values of the physical parameters are $\varepsilon_g=0.3$; $\rho_g=1400$ kg/m^3; $\xi=1.5\times10^{17}$ m^{-2}; $D=2.2\times10^{-12}$ m^2/s, and $c_g/c_0=3.2$ for PEEK-WC hollow fiber membrane [4.6 in case of PSU membrane]).

on the temperature of the system, higher the temperature more is the diffusivity. Effects of gel layer concentration on flux are observed by comparing Curves 2 and 3. As presented in theoretical section, the effect of C_g on flux is marginal (Eq. 19). The value of gel layer resistance parameter ξ has strong influence on steady-state flux as can be seen from Curves 2 and 4. As this parameter decreases one order of magnitude, the permeate flux increases from 120 to 280 L/m^2 h at $Re=5000$ as expected. The variation of gel layer thickness at steady state with Reynolds number is described in Figure 5b. With increase in forced convection (or turbulence), the gel layer thickness decreases and this is clear from all the curves in Figure 5b. Comparing Curves 1 and 4, the effect of ξ is shown on the gel layer thickness. As the gel resistance parameter ξ is decreased from 10^{17} to 10^{16} m^{-2}, the gel thickness increases three folds. However, it must be clarified here, that apparently one would expect higher permeate flux when gel thickness decreases and likewise the permeate flux corresponding to Curve 1 (high ξ) is expected to be more than Curve 4 (low ξ). But, as already shown in the previous figure, permeate flux increases with decrease in the magnitude of ξ. It may be noted that the gel layer resistance is dependent on both gel resistance parameter (ξ) and gel thickness (H). Thus, the effect of ξ surpasses that of gel layer thickness, H, leading to decrease in permeate flux (Figure 5a). The effect of c_g/c_0 on the gel layer thickness is more prominent (Curves 1 and 3) than that on the steady-state flux.

The validation of the developed model is illustrated in Figure 6 using the optimized values of the physical parameters. Membrane specifications and experimental conditions are already stated in Tables 1 and 3. The optimized set of parameters are $\varepsilon_g=0.3$; $\rho_g=1400$ kg/m^3; $\xi=1.5\times10^{17}$ m^{-2}; $D=2.2\times10^{-12}$ m^2/s, and $c_g/c_0=3.2$ (4.6 in case of PSU membrane). The model results show that the permeate flux values are well within ±10% of the experimental data. Two additional set of simulated flux profiles corresponding to twice the cross flow velocity as used in the experiment were also presented in figure (dotted lines). It is understood from this figure that gel layer resistance has major contribution to the flux decline behavior. The steady-state flux is reduced to 25% of its pure water flux. Noting the optimized values of c_g/c_0 for different membranes, it can be inferred that with increase in membrane hydrophilicity, the magnitude of c_g/c_0 decreases.

Batch concentration mode

The same set of parameter values as obtained from the total recycle mode calculation are used for prediction of the batch mode filtration performance. The permeate flux profile with varying Reynolds number is presented in Figure 7. It is observed from the figure, that upto 3 h, permeate flux is more at higher Reynolds number. This effect becomes marginal after that. As discussed earlier, gel layer thickness is less at higher Reynolds number, leading to increase in permeate flux. However, under batch mode of filtration, more be the permeate flux at higher Re number, the feed becomes concentrated further. Increase in feed concentration leads to enhanced deposition of solute particles over the membrane surface, thereby increasing the gel layer thickness. This finally results to decline in permeate flux. It is apparent from Figure 7 that beyond 3 h of operation, the effect of concentration of feed becomes dominant compared to that of enhanced turbulence. This explains the trends of curves in Figure 7 beyond 3 h. For example, the curve corresponding to $Re=7000$ has reversed after 3 h, representing minimum value of permeate flux among three Re number. The feed concentration effect on gel thickness is demonstrated in the inset of Figure 7. For initial 3 h of filtration, the gel thickness does not change appreciably with Reynolds number. However, beyond 3 h of operation, the thickness of the gel layer increases with turbulence in the flow profile due to enhanced feed concentration, and

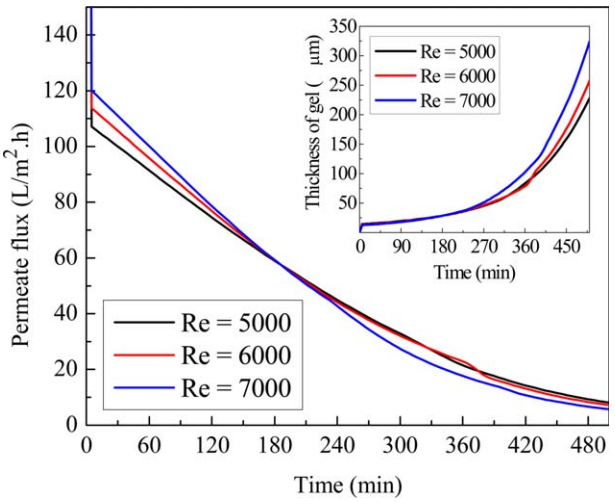

Figure 7. Permeate flux profile with variation of Reynolds number in Batch mode of operation; inset: Growth of gel layer thickness with time of filtration (PEEK-WC membrane and values of the physical parameters are $\rho_g=1400$ kg/m^3; $\varepsilon_g=0.3$; $D=5\times10^{-11}$ m^2/s; $C_g=3.2$; $\xi=1.5\times10^{17}$ m^{-2}).

[Color figure can be viewed in the online issue, which is available at wileyonlinelibrary.com.]

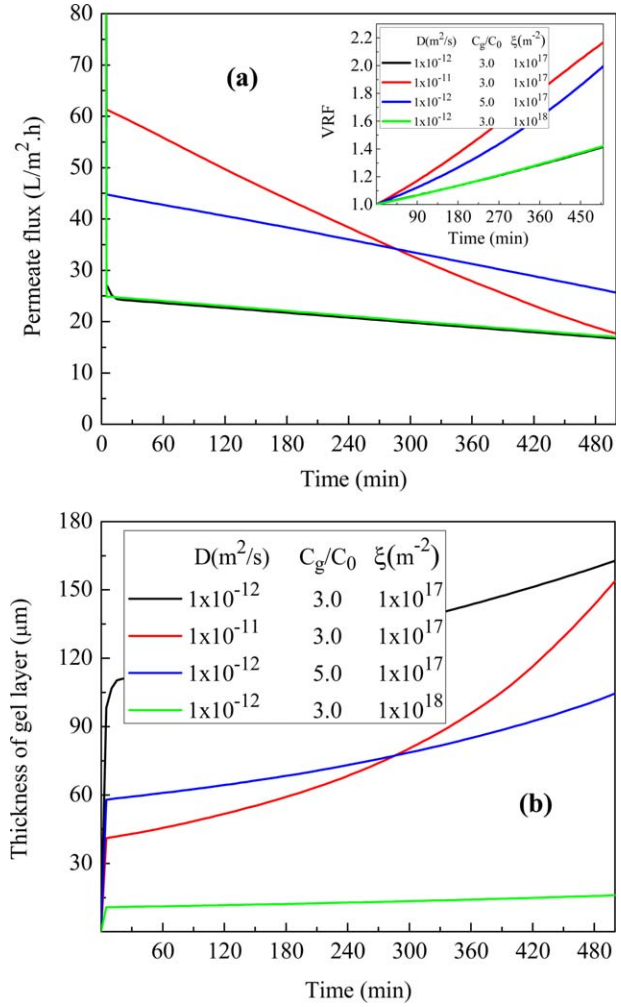

Figure 8. (a) Flux decline profile for various combinations of parameters in batch mode; inset: profile of VRF for different variation of the physical parameters (PEEK-WC membrane and values of the physical parameters are $\rho_g = 1400$ kg/m^3; $\varepsilon_g = 0.3$). (b) Growth of gel layer for batch mode of filtration with different combination of physical parameters (PEEK-WC membrane and values of the physical parameters are $\rho_g = 1400$ kg/m^3; $\varepsilon_g = 0.3$).

[Color figure can be viewed in the online issue, which is available at wileyonlinelibrary.com.]

consequently the permeate flux decreases. Thus, there exists a transition time, 3 h for MF of pomegranate juice in hollow fiber, after which the gel layer thickness becomes significantly high and gel resistance becomes more dominant due to increase in feed concentration compared to turbulence in flow channel.

The effect of the physical parameters on the filtration performance in illustrated in Figure 8a. It can be seen that permeate flux and also its rate of reduction increases with diffusivity (comparing red and black curves) and gel concentration C_g (comparing blue and black curves). In case of increase in the gel layer resistance parameter (ξ) from 10^{17} to 10^{18} m^{-2}, there is hardly any change in the permeate flux. In fact, the green and black curves almost superimpose each other. The magnitude of ξ strongly influences the gel layer thickness. However, in the case of batch mode of filtration, the change in concentration of feed dominates the gel layer thickness and consequently, the flux decline mechanism. The corresponding effect of these parameters on the volume reduction is shown in the inset. The trend in the rise of VRF is perfectly in accordance with Eqs. 32 and 34. The trends of profiles of permeate flux and VRF with other parameters, D and c_g/c_0 shows expected behavior. The development of the gel layer thickness for different combination of the physical constants is presented in Figure 8b. The gel layer thickness decreases with increase in diffusivity (compare black and red curves). With increase in diffusivity, more solutes diffuse back from the gel layer to the bulk of the solution. This reduces the gel layer thickness as observed in this figure. However, these two curves approach each other with progress of filtration. This is due to the fact

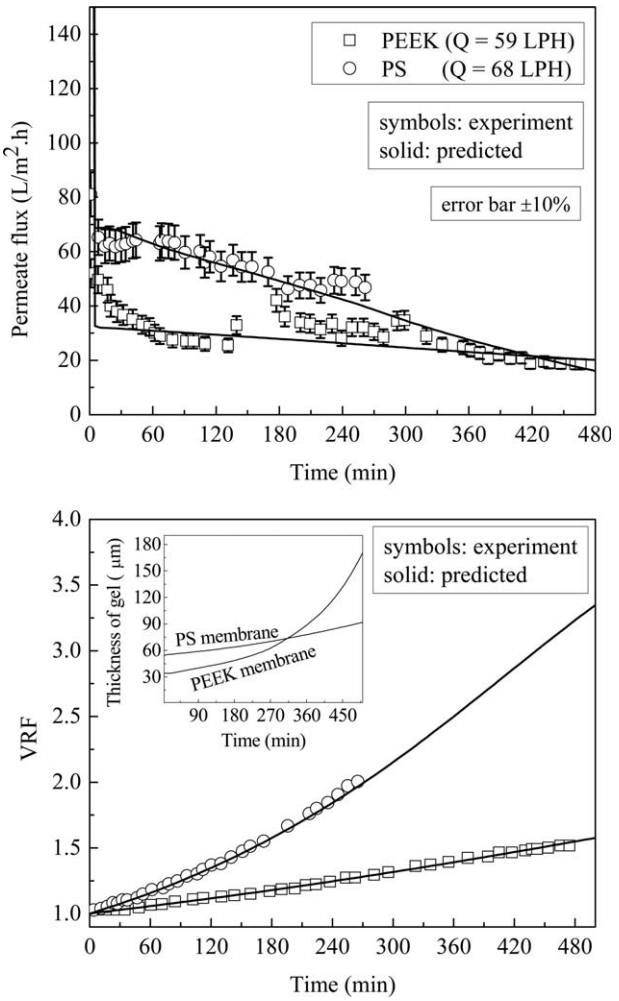

Figure 9. (a) Comparison of the experimental and predicted flux profiles for batch mode filtration (the values of the physical parameters are those optimized in total recycle mode). (b) Comparison of the experimental and predicted VRF profiles for different membrane systems; inset: Gel layer dynamics for this operating condition corresponding to the experimental results (the values of the physical parameters are those optimized in total recycle mode).

that the permeate flux increases with enhanced diffusivity resulting to increase in concentration in the feed as discussed earlier. In fact, this effect becomes more dominant and the gel layer thickness increases rapidly with time. Effects of c_g/c_0 on gel layer thickness are observed by comparing black and blue curves. Gel layer thickness is less for higher gel concentration. For a constant feed concentration, more solutes are required to form gel and gel formation is hindered resulting to diminished gel thickness. Comparison of black and green curves shows the effect of ξ on gel layer thickness. As ξ increases, the gel becomes more compact leading to its reduced thickness. It may be noted that even though ξ has a pronounced effect on gel thickness, its effect on permeate flux is marginal as discussed in the preceding section.

Finally, the comparison of the predicted model results with experimental data is presented in Figure 9. The values of the model parameters, as obtained by optimizing the flux profiles in case of total recycle mode of operation, are used to predict the performance of batch mode of operation. The experiment is conducted upto 4 h, in case of PSU membrane. However, the model results are extended for 8 h. It can be seen that for most of the data points, the model results are within $\pm 10\%$ of the experimental results. In case of profiles for the VRF, the model prediction is almost equal to the experimental results. The results of batch mode suggests that for different operating conditions, the permeate flux approaches to a limiting value after a considerable time of operation. Similar to the total recycle mode operation, the flux reduces to almost 10% of the pure water flux. The transient profile of the gel layer thickness is obtained from the simulation as shown in Figure 9b. This suggests that in case of PEEK-WC membrane, the development of the gel layer is sharper compared to PSU membrane.

Summary and Conclusions

Interplay of various solute and gel layer characteristic parameters on the dynamics of gel formation and flux decline has been analyzed in turbulent flow in hollow fiber during cross flow MF of fruit juice through a model developed from first principles. The major conclusions from this study are summarized below.

1. The optimized physicochemical parameters for the gel and solutes were: $\varepsilon_g=0.3$; $\rho_g=1400$ kg/m^3; $\xi=1.5\times10^{17}$ m^{-2}; $D=2.2\times10^{-12}$ m^2/s, and $c_g/c_0=3.2$ for PEEK-WC hollow fiber membrane (4.6 in case of PSU hollow fiber membrane).

2. Under the total recycle mode of filtration, the gel layer thickness decreases with turbulence. It decreases from 7.5 to 4 μm as Re increases from 5000 to 15,000 at the end of the module. Consequently, Sherwood number increases from 250 to 550 resulting in increase of permeate flux.

3. Gel resistance parameter ξ had the dominant effect on steady-state permeate flux. At $Re=5000$, permeate flux increases by 5.5 times.

4. Among the gel resistance parameter (ξ) and gel thickness (H), ξ has stronger effect on gel resistance and hence permeate flux.

5. In case of batch mode of filtration, effect of turbulence was dominant on permeate flux decline upto 3 h and the effect of concentration of feed becomes significant beyond that.

6. Gel concentration has stronger effect on gel thickness compared to permeate flux. Gel layer thickness was less at higher gel concentration.

7. The model successfully predicted the performance of batch mode of filtration and the agreement with experimental data was within $\pm5\%$.

8. The present modeling work can further help in scale-up and process design of the system. (a) Dealing with high throughput, the profile of flux decline can be closely followed so that permeate flux does not fall below a limit, which is not economically feasible. (b) The time of filtration, and onset of cleaning protocol can be inferred from this study. (c) The maximum achievable VRF and its interrelation with permeate quality can also be interpreted from such analysis. (d) For a large throughput system, the required membrane area can also be estimated. For example, to have 200 L/h process output, one would require a membrane area of 4.4 m^2. (e) Influence of polymeric membrane material on system performance is also observed. The PSU membrane shows higher permeate flux decline compared to PEEK-WC membrane.

Acknowledgments

This work is partially supported by a grant from the Board of Research in Nuclear Sciences, Department of Atomic Energy, Government of India, Mumbai, under the scheme no. 2012/21/03-BRNS, Dt. 25-07-2012. Any opinions, findings and conclusions expressed in this paper are those of the authors and do not necessarily reflect the views of BRNS.

Notation

a_0, a_1, a_2 = coefficients in Eq. 8
A_m = membrane Area, m^2
c = concentration, kg/m^3
C = nondimensional concentration, c/c_0
c_0 = initial concentration, kg/m^3
c_b = concentration in batch mode, kg/m^3
c_g = gel layer concentration, kg/m^3
C_g = nondimensional gel layer concentration, c_g/c_0
c_p = permeate concentration, kg/m^3
D = diffusivity, m^2/s
Err = relative error between experimental and predicted fluxes
H = height of the gel layer in total recycle mode, m
H_{ss} = thickness of gel layer at steady state, m
H_b = height of the gel layer in batch concentration mode, m
I_1 = integral in Eq. 12
$\overline{k_L}$ = length averaged mass-transfer coefficient, m/s
L = length of the hollow fiber tubule, m
n = number of fibers in a hollow fiber module
P = nondimensional constant in Eq. 6
Pe_w = nondimensional permeate flux
Q = nondimensional constant in Eq. 6
Q_F = volumetric cross flow rate, m^3/s
r = local radial co-ordinate, m
R = nondimensional constant in Eq. 6
Re = Reynolds number at the module entrance
R_g = gel layer constant, m^{-1}
R_m = membrane hydraulic constant, m^{-1}
S = nondimensional constant in Eq. 6
Sc = Schmidt number
Sh = Sherwood number
Sh_L = length averaged Sherwood number
T = nondimensional constant in Eq. 6
t = time of filtration, min
U = nondimensional constant in Eq. 6
u^* = shear velocity, m/s
u^+ = nondimensional velocity

u_0 = linear velocity in a tube corresponding to Q_F, m/s
v = velocity y-component, m/s
V = volume, m^3
V_0 = initial feed volume in batch concentration mode, m^3
v_w = permeation velocity, m/s
y = local y-coordinate, m
Y = nondimensional y-coordinate
y^+ = near wall co-ordinate system, m

Greek letters

β = specific gel layer resistance constant, m/kg
δ = mass transfer boundary layer thickness, m
Δ = nondimensional mass transfer boundary layer thickness
ΔP = transmembrane pressure drop, kPa
ε_g = gel layer porosity
λ = Von-karman constant equal to 0.41
μ = viscosity of the solution, Pa s
ρ = solution density, kg/m^3
ρ_f = solution density of feed, kg/m^3
ρ_g = gel layer density, kg/m^3
ρ_p = solution density of permeate, kg/m^3
τ_w = wall shear stress, Pa
ξ = gel layer resistance parameter, m^{-2}

Literature Cited

1. Rai P, Rai C, Majumdar GC, Das Gupta S, De S. Storage study of ultrafiltered mosambi (Citrus sinensis [L.] Osbeck) juice. *J Food Process Preserv*. 2008;32:923–934.
2. Rai P, Majumdar GC, DasGupta S, De S. Effect of various pretreatment methods on permeate flux and quality during ultrafiltration of mosambi juice. *J Food Eng*. 2007;78:561–568.
3. Rai P, Majumdar GC, Sharma G, DasGupta S, De S. Effect of various cutoff membranes on permeate flux and quality during filtration of mosambi (Citrus sinensis L.) Osbeck juice. *Food Bioprod Process*. 2006;84:213–219.
4. Vladisavljević GT, Vukosavljević P, Bukvić B. Permeate flux and fouling resistance in ultrafiltration of depectinized apple juice using ceramic membranes. *J Food Eng*. 2003;60:241–247.
5. De Bruijn JPF, Vanegas A, Martinez JA, Bórquez R. Ultrafiltration performance of Carbosep membranes for the clarification of apple juice. *LWT-Food Sci Technol*. 2003;36:397–406.
6. Tanada-Palmu P, Jardine J, Matta V. Oriduction of banana (Musa cavendishii) extract containing no polyphenol oxidase by ultrafiltration. *J Sci Food Agric*. 1999;79:643–647.
7. Jiraratananon R, Chanachai A. A study of fouling in the ultrafiltration of passion fruit juice. *J Membr Sci*. 1996;111:39–48.
8. Balakrishnan M, Dua M, Bhagat JJ. Effect of operating parameters on sugarcane juice ultrafiltration: results of field experience. *Sep Purif Technol*. 2000;19:209–220.
9. De Barros STD, Andrade CMG, Mendes ES, Peres L. Study of fouling mechanism in pineapple juice clarification by ultrafiltration. *J Membr Sci*. 2003;215:213–224.
10. Laorko A, Li Z, Tongchitpakdee S, Chantachum S, Youravong W. Effect of membrane property and operating conditions on phytochemical properties and permeate flux during clarification of pineapple juice. *J Food Eng*. 2010;100:514–521.
11. Hernandez E, Chen CS, Shaw PE, Carter RD, Barros S. Ultrafiltration of orange juice: effect on soluble solids, suspended solids, and aroma. *J Agric Food Chem*. 1992;40:986–988.
12. Cassano A, Marchio M, Drioli E. Clarification of blood orange juice by ultrafiltration: analyses of operating parameters, membrane fouling and juice quality. *Desalination*. 2007;212:15–27.
13. Cassano A, Conidi C, Timpone R, D'Avella M, Drioli E. A membrane-based process for the clarification and the concentration of the cactus pear juice. *J Food Eng*. 2007;80:914–921.
14. Cassano A, Drioli E, Galaverna G, Marchelli R, Di Silvestro G, Cagnasso P. Clarification and concentration of citrus and carrot juices by integrated membrane processes. *J Food Eng*. 2003;57:153–163.
15. Cassano A, Donato L, Drioli E. Ultrafiltration of kiwifruit juice: operating parameters. *Juice quality and membrane fouling*. *J Food Eng*. 2007;79:613–621.
16. Baklouti S, Ellouze-Ghorbel R, Mokni A, Chaabouni S. Clarification of pomegranate juice by ultrafiltration: study of juice quality and of the fouling mechanism. *Fruits*. 2012;67:215–225.
17. Mirsaeedghazi H, Mousavi SM, Emam-Djomeh Z, Rezaei K, Aroujalian A, Navidbakhsh M, Comparison between ultrafiltration and microfiltration in the clarification of pomegranate juice. *J Food Process Eng*. 2012;35:424–436.
18. Mondal S, Cassano A, Tasselli F, De S. A generalized model for clarification of fruit juice during ultrafiltration under total recycle and batch mode. *J Membr Sci*. 2011;366:295–303.
19. De S, Bhattacharya PK. Prediction of mass-transfer coefficient with suction in applications of reverse osmosis and ultrafiltration. *J Membr Sci*. 1997;128:119–131.
20. Yeh HM, Cheng TW. Osmotic pressure model with permeability analysis for ultrafiltration in hollow-fiber membrane modules. *Sep Technol*. 1993;3:91–98.
21. Parvatiyar MG. Mass transfer in a membrane tube with turbulent flow of Newtonian and non-Newtonian fluids. *J Membr Sci*. 1998; 148:45–57.
22. Minikanti VS, Dasgupta S, De S. Prediction of Mass transfer coefficient with suction for turbulent flow in cross flow ultrafiltration. *J Membr Sci*. 1999;157:227–239.
23. Ranjan R, Dasgupta S, De S. Mass transfer coefficient with suction for turbulent non-Newtonian flow in application to membrane separation. *J Food Eng*. 2004;65:533–541.
24. Sreenivas K, Ragesh P, Dasgupta S, De S. Modeling of cross-flow pressure controlled membrane separation processes under turbulent flow conditions. *J Membr Sci*. 2002;201:203–212.
25. Bird RB, Stewart WE, Lightfoot EN. *Transport Phenomena*, *2nd ed*. New York: Wiley, 2007.
26. Reichardt H. Vollständige Darstellung der turbulenten Geschwindigkeitsverteilung in glatten Leitungen. *J Appl Math Mech*. 1951;31: 208–219.
27. Fox RW, McDonald AT. *Introduction to Fluid Mechanics*, *5th ed*. New Delhi, India: Wiley, 2004.
28. Lévêque A. Les lois de la transmission de chaleur par convection. *Ann Mines*. 1928;13:201–299.
29. De S, Bhattacharya S, Sharma A, Bhattacharya PK. Generalized integral and similarity solutions for concentration profiles for osmotic pressure controlled ultrafiltration. *J Membr Sci*. 1997;130: 99–121.
30. Mondal S, Rai C, De S. Modeling of cross flow ultrafiltration of stevia extract in a rectangular cell. *J Food Eng*. 2012;112:326–337.
31. Byrd RH, Gilbert JC, Nocedal J. A trust region method based on interior point techniques for nonlinear programming. *Math Program*. 2000;89:149–185.
32. Coleman TF, Li Y. An interior, trust region approach for nonlinear minimization subject to bounds. *SIAM J Optim*. 1996;6:418–445.
33. Tasselli F, Cassano A, Drioli E. Ultrafiltration of kiwifruit juice using modified poly(ether ether ketone) hollow fibre membranes. *Sep Purif Technol*. 2007;57:94–102.
34. Song W, Ravindran V, Koel BE, Pirbazari M. Nanofiltration of natural organic matter with H2O2/UV (hydrogen peroxide-ultraviolet radiation) pretreatment: fouling mitigation and membrane surface characterization. *J Membr Sci*. 2004;241:143–160.
35. Crozes G, Anselme C, Mallevialle J. Effect of adsorption of organic matter on fouling of ultrafiltration membranes. *J Membr Sci*. 1993; 84:61–77.
36. Williams ME, Hestekin JA, Smothers CN, Bhattacharyya D. Separation of organic pollutants by reverse osmosis and nanofiltration membranes: mathematical models and experimental verification. *Ind Eng Chem Res*. 1999;38:3683–3695.
37. Mondal S, De S. Generalized criteria for identification of fouling mechanism under steady state membrane filtration. *J Membr Sci*. 2009;344:6–13.
38. Mondal S, De S. A fouling model for steady state crossflow membrane filtration considering sequential intermediate pore blocking and cake formation. *Sep Purif Technol*. 2010;75:222–228.
39. Tu CS, Ravindran R, Den W, Pirbazari M. Predictive membrane transport model for nanofiltration in water treatment applications. *AIChE J*. 2001;47:1346–1362.
40. Tu SC, Ravindran V, Pirbazari M. A pore diffusion model for forecasting the performance of membrane processes. *J Membr Sci*. 2005; 265:29–50.
41. Williams MD, Pirbazari M. Membrane bioreactor process for removing biodegradable organic matter from water. *Water Res*. 2007;41: 3880–3893.
42. Williams MD, Ravindran V, Pirbazari M. Modeling and process evaluation of membrane bioreactor for removing biodegradable organic matter from water. *Chem Eng Sci*. 2012;84:494–511.

43. Escobar IC, Randall AA, Taylor JS. Bacterial growth in distribution systems: effect of assimilable organic carbon and biodegradable organic carbon. *Environ Sci Technol.* 2001;35: 3442–3447.

44. Escobar IC, Hong SK, Randall AA. Removal of assimilable organic carbon and biodegradable dissolved organic carbon by reverse osmosis and nanofiltration membranes. *J Membr Sci.* 2000;175:1–17.

APPENDIX A

The integral I_1 obtained in Eq. 12 can be expanded as

$$I_1=\underbrace{\frac{P}{\Delta^2}\int_0^{\Delta}Y\ln(1+QY)dY}_{I_2}-\underbrace{\frac{P}{\Delta^3}\int_0^{\Delta}Y^2\ln(1+QY)dY}_{I_3}+\underbrace{R\int_0^{\Delta}\left(\frac{Y}{\Delta^2}-\frac{Y^2}{\Delta^3}\right)dY}_{I_4}$$
$$-\underbrace{R\int_0^{\Delta}\exp(-SY)\left(\frac{Y}{\Delta^2}-\frac{Y^2}{\Delta^3}\right)dY}_{I_5}-\underbrace{RS\int_0^{\Delta}Y\exp(-TY)\left(\frac{Y}{\Delta^2}-\frac{Y^2}{\Delta^3}\right)dY}_{I_6} \tag{A1}$$

Therefore,

$$I_1=I_2-I_3+I_4-I_5-I_6 \tag{A2}$$

Integrating each of the individual terms in the range 0 to Δ we get

$$I_2=\frac{P}{Q^2\Delta^2}\left[\left\{\frac{1}{2}(1+Q\Delta)^2-(1+Q\Delta)\right\}\ln(1+Q\Delta)-\frac{1}{4}(1+Q\Delta)^2+Q\Delta+\frac{1}{4}\right] \tag{A3}$$

$$I_3=\frac{P}{Q^3\Delta^3}\left[\left\{\frac{1}{3}(1+Q\Delta)^3-(1+Q\Delta)^2+(1+Q\Delta)\right\}\ln(1+Q\Delta)-\frac{1}{9}(1+Q\Delta)^3+\frac{1}{2}(1+Q\Delta)^2-Q\Delta-\frac{7}{18}\right] \tag{A4}$$

$$I_4=\frac{R}{6} \tag{A5}$$

$$I_5=\frac{1}{S\Delta^3}\left[\frac{2}{S^2}-\exp(-S\Delta)\left\{\Delta^2+\frac{2\Delta}{S}+\frac{2}{S^2}\right\}\right]+\frac{1}{S\Delta^2}\left[\frac{1}{S}-\exp(-S\Delta)\left\{\Delta+\frac{1}{S}\right\}\right] \tag{A6}$$

$$I_6=\frac{RS}{T\Delta^2}\left[\frac{2}{T^2}-\exp(-T\Delta)\left\{\Delta^2+\frac{2\Delta}{T}+\frac{2}{T^2}\right\}\right]-\frac{RS}{T\Delta^2}\left[\frac{6}{T^3}-\exp(-T\Delta)\left\{\Delta^3+\frac{3\Delta^2}{T}+\frac{6\Delta}{T^2}+\frac{6}{T^3}\right\}\right] \tag{A7}$$

APPENDIX B

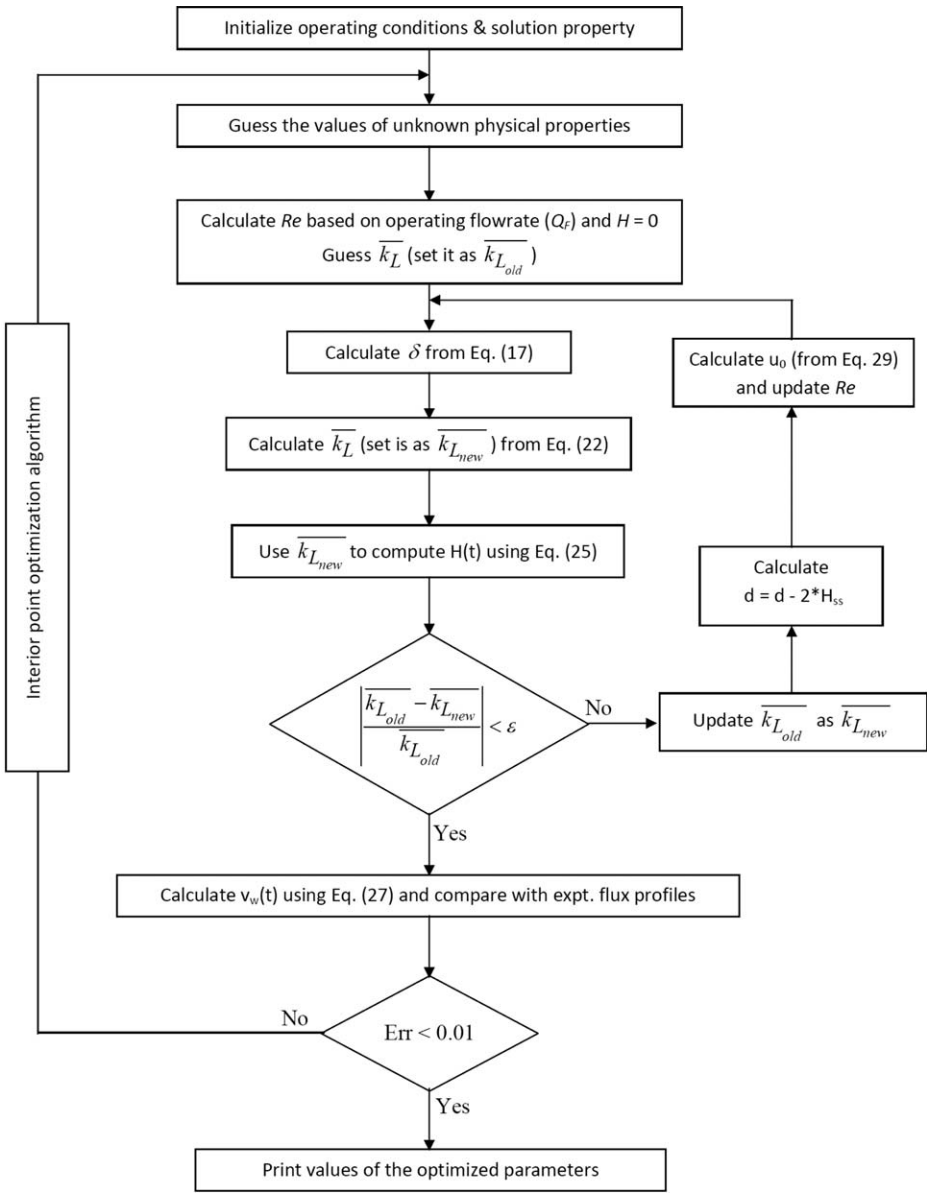

Manuscript received Apr. 24, 2014, and revision received July 11, 2014.